Supporting Information

Thomas *et al.* 10.1073/pnas.0804249105

SI Methods

Cell Cycle Analysis. The effects of HDACi 4b on cell cycle progression were monitored by flow cytometry analysis in the Scripps FACS core facility. Cultured EBV transformed lymphoblast cells (GM15850 from the National Institute of General Medical Sciences Human Genetic Cell Repository at the Coriell Institute, Camden, New Jersey) were cultured in Roswell Park Memorial Institute medium 1640 containing 15% FBS as recommended by Coriell. Untreated, 0.1% DMSO, and 4b-treated (5–125 μM) cells were cultured for 24 h before collection by centrifugation (150 $\times$ *g* for 10 min). Cell pellets were resuspended in 500 μl of PBS and fixed with the addition of 4.5 ml of prechilled 70% ethanol, stained with propidium iodide (50 μg/ml), and analyzed for DNA content. The fraction of cells at each point in the cell cycle (Apo, G1, S, and G2/M) was measured on the basis of 2C and 4C DNA populations of the gated cells. Apoptosis is assumed for cells with less than a 2C DNA content, indicative of fragmentation.

Rotarod and Behavioral Semiquantitative Assessment of Motor and Postural Dysfunction. Mice were tested on an AccuRotor rotarod (AccuScan Instruments) during the light phase of the 12-h light/dark cycle using an accelerating rotation paradigm (4–20 rpm). Mice were trained on the rotarod before drug treatment (3 months of age) to establish a behavioral baseline. Baseline training involved 3 consecutive days of nine trials in three sets of three, with 1 min between each test within a set and approximately 1 h between each set. During the drug treatment duration, mice were tested in a single set of three trials, to assess motor coordination changes associated with disease progression and the effects of drug treatment.

Behavioral semiquantitative assessment of motor and postural abnormalities were scored according to an adaptation of a previously described motor scale, including the following items, which constitute the main motor symptoms observed: hindlimb clasping, reduced global activity in a freely moving environment, hindlimb dystonia, and truncal dystonia (kyphosis) (1, 2). Mice were placed in Plexiglas cages (42 $\times$ 22 $\times$ 20 cm) and observed for 10-min sessions, in which each test was rated (0–4) according to the following scoring criteria.

Hindlimb clasping. Each mouse is suspended by its tail for 30 sec 10 cm above the ground and scored as follows: 0, normal hindlimb movements (hindlimbs are fully spread and moving about); 1–2, intermittent clasping of one hindlimb; 3, intermittent clasping of both hindlimbs; 4, both hindlimbs are fully drawn up to the abdomen.

General locomotor activity. Mice are scored for displacement velocity, exploratory behavior, rearing, and grooming as follows: 0, normal; 1–2, slight reduction of general activity (displacement velocity, rearings, and grooming are reduced); 3, reduction in general activity (very little rearing or grooming); 4, marked reduction of general activity (the mouse stays in place or moves very slowly with no rearing or grooming).

Truncal dystonia. The flexed kyphotic posture of each mouse is assessed as follows: 0, absent; 1–2, slightly flexed with visible kyphosis; 3, visible kyphosis; 4, markedly abnormal flexed posture with severe kyphosis.

Assessments were made by two independent observers who were blind to genotype and treatment status.

Microarray Data Concordance. We assessed the correlation between gene expression changes detected in R6/2^{290Q} transgenic mice compared with those observed in human HD by calculating the concordance coefficient, *c*, exactly as described previously (3). The concordant regulation was defined as a pair of orthologous probe sets reporting same-direction differential expression between disease and control (i.e., both upregulated or both downregulated) whereby the human probe set showed a significant expression change (FDR $<$ 0.05) (4). Similarly, discordant regulation was defined as two probe sets reporting opposite sign regulations whereby the human probe set showed a significant expression change (FDR $<$ 0.05). The concordance coefficient, *c*, was defined as:

$$c = \frac{\#\text{concordant} - \#\text{discordant}}{N}$$

where #concordant is the number of concordant orthologous probe set pairs, #discordant the number of discordant orthologous probe set pairs, and *N* the number of mouse probe sets selected for the comparison. Of the top 250 differentially expressed genes in mouse, 10 gene IDs had no human homologue, and 10 other gene IDs that had human homologues were not on the Illumina arrays, leaving 230 genes for the comparison.

Real-Time PCR Analysis. Real-time PCR experiments were performed using the ABI PRISM 7900HT Sequence Detection System (Applied Biosystems). Amplification was performed on a cDNA amount equivalent to 25 ng total RNA with 1$\times$ SYBR Green universal PCR Master mix (Applied Biosystems) containing deoxyribonucleotide triphosphates, $MgCl_2$, AmpliTaq Gold DNA polymerase, and forward and reverse primers. PCR reactions were performed on four independent sets of template from the cerebellum and striatum of vehicle- and HDACi 4b–treated WT and R6/2^{300} transgenic mice. Specific primers for each sequence were designed using Primer Express 1.5 software, and their specificity for binding to the desired sequences was searched against the National Center for Biotechnology Information database (Table S2). Standard curves were generated for each gene of interest using serial dilutions of mouse cDNAs. Experimental samples and no-template controls were all run in duplicate. The PCR cycling parameters were: 50°C for 2 min, 95°C for 10 min, and 40 cycles of 94°C for 15 s, 60°C for 1 min. Finally, a dissociation protocol was also performed at the end of each run to verify the presence of a single product with the appropriate melting point temperature for each amplicon. The amount of cDNA in each sample was calculated using SDS2.1 software by the comparative threshold cycle (Ct) method and expressed as 2exp(Ct) using hypoxanthine guanine phosphoribosyl transferase as an internal control. For calculations applying the Ct method, vehicle-treated WT mice expression values were used as calibrator samples standardized to the value of 1.

1. Fernagut PO, *et al.* (2002) Subacute systemic 3-nitropropionic acid intoxication induces a distinct motor disorder in adult C57Bl/6 mice: Behavioural and histopathological characterisation. *Neuroscience* 114:1005–1017.
2. Diguet E, *et al.* (2004) Deleterious effects of minocycline in animal models of Parkinson's disease and Huntington's disease. *Eur J Neurosci* 19:3266–3276.
3. Kuhn A, *et al.* (2007) Mutant huntingtin's effects on striatal gene expression in mice recapitulate changes observed in human Huntington's disease brain and do not differ with mutant huntingtin length or wild-type huntingtin dosage. *Hum Mol Genet* 16:1845–1861.
4. Hodges A, *et al.* (2006) Regional and cellular gene expression changes in human Huntington's disease brain. *Hum Mol Genet* 15:965–977.

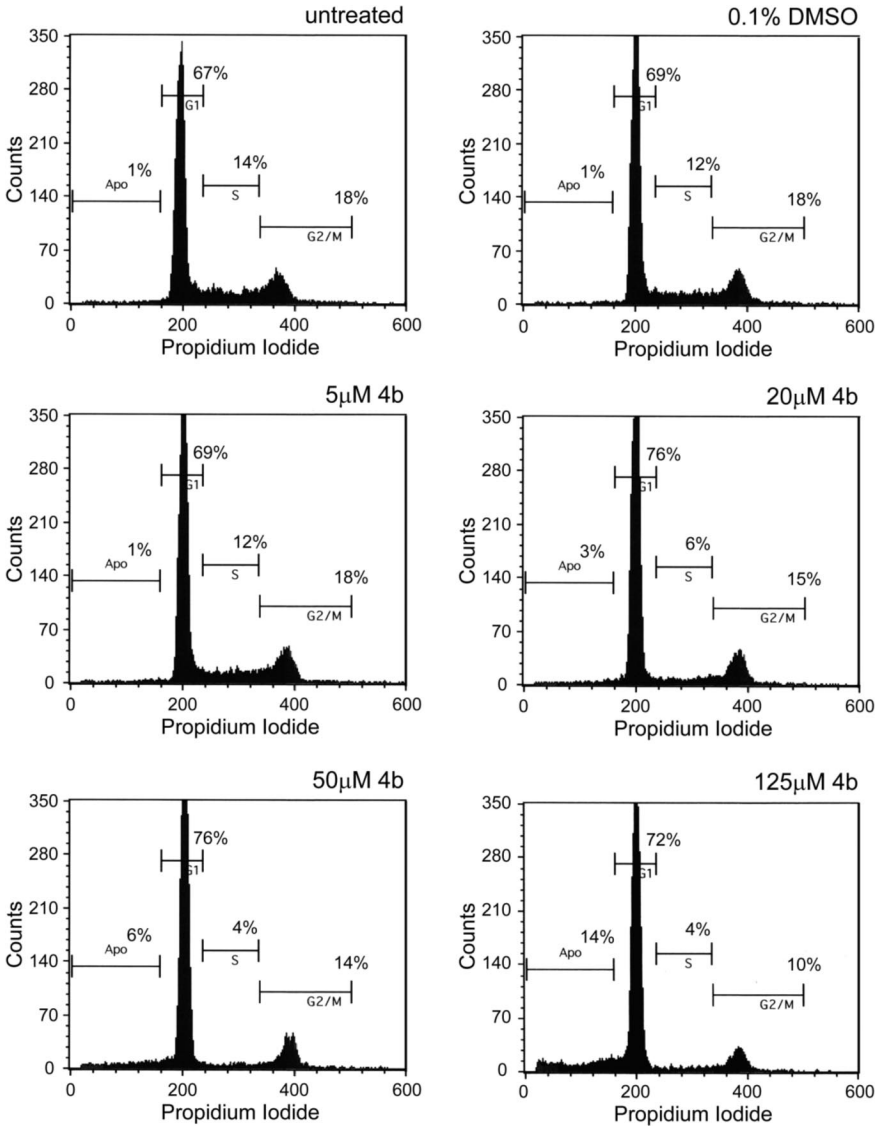

Fig. S1. The effects of HDACi 4b on cell cycle populations in cultured lymphoblasts. FACS analysis of propidium iodide-stained fixed cells after 24 h incubation of indicated condition (above the upper right hand corner of each graph) was performed as described in *SI Methods*. 1E5 cells were measured, and populations (%) are given above each gate for apoptosis (Apo), G1, S, and G2/M.

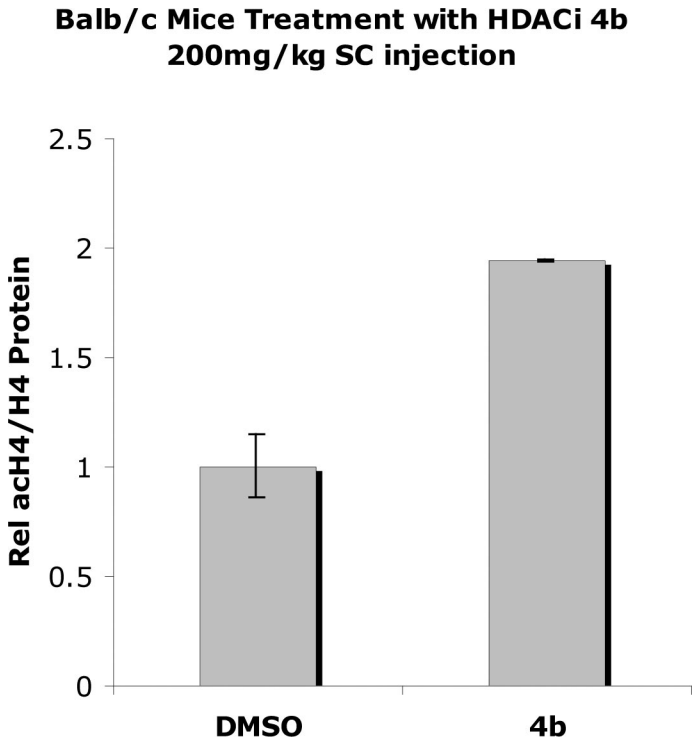

Fig. S2. HDACi 4b treatment increases histone acetylation in the brain. BALB/c mice were injected with HDACi 4b (200 mg/kg, dissolved in DMSO) or vehicle (50 μl DMSO) and killed after 6 h. Western blot analysis was performed on whole-brain homogenates from $n = 2$ mice per condition using the histone-specific antibodies Histone H4 (Abcam 10158) and AcHistone H4 (Cell Signaling Technologies 06598).

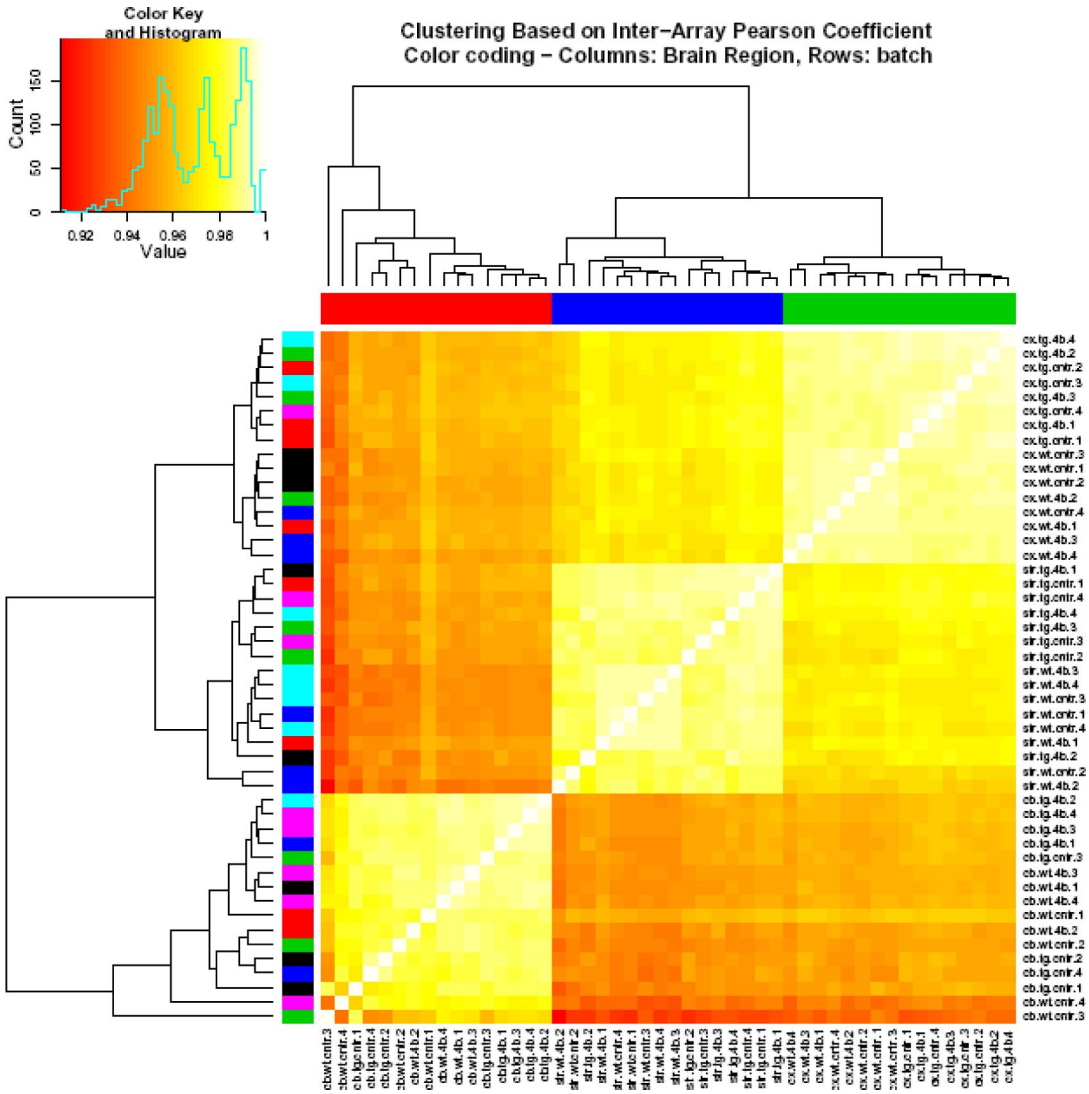

Fig. S3. Hierarchal clustering of the samples based on interarray Pearson correlation.

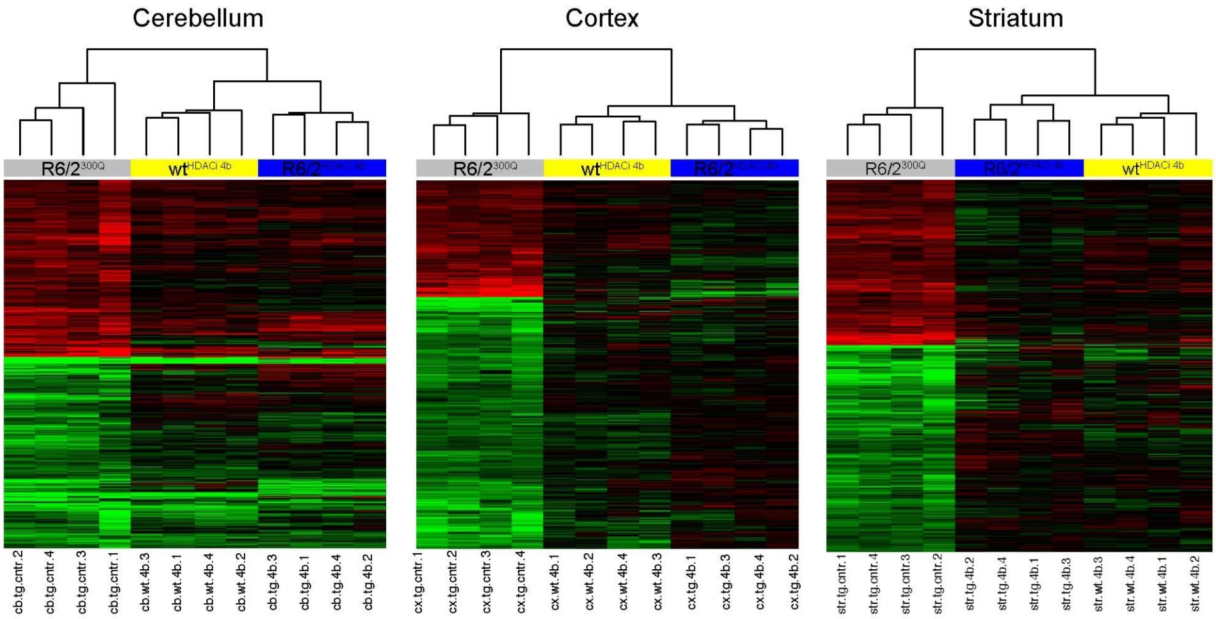

Fig. S4. Heatmaps depicting the probes that are differentially expressed in R6/2^{300Q} vs. WT mice ($P < 0.005$, gray bar) and in HDACi 4b-treated vs. untreated R6/2^{300Q} transgenic mice ($P < 0.005$, blue bar). The HDACi 4b effect on WT mice in these genes is marked by the yellow bars. Log_2-transformed ratios were subjected to two-dimensional hierarchical clustering. Each colored pixel represents an individual ratio from a single subject (four replicates per condition) compared with the average of controls. Relative decreases in gene expression are indicated by green and increases in expression by red.

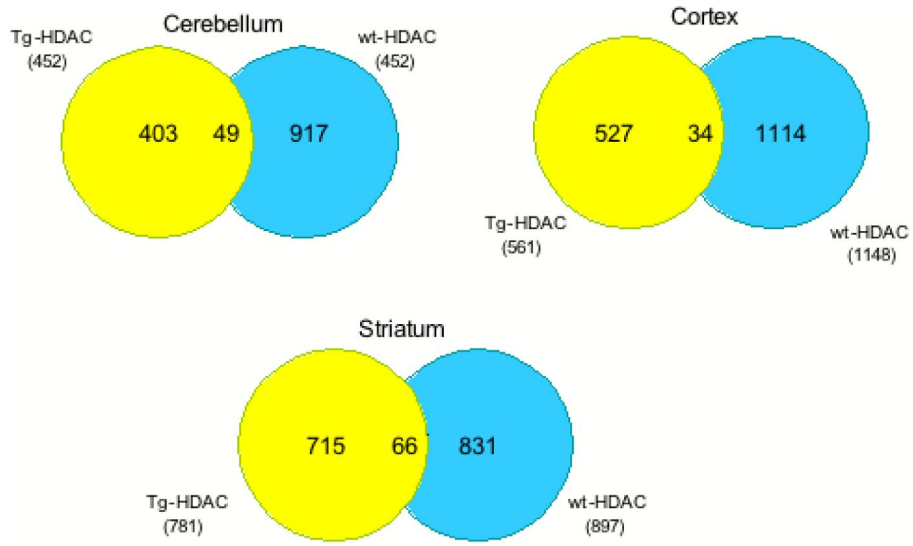

Fig. S5. Overlap of HDACi 4b-induced gene expression changes in striatum, cortex, and cerebellum of WT vs. R6/2^{Q290} transgenic mice. The numbers in the green portions of the Venn diagrams represent those gene expression changes induced by HDACi 4b treatment in both WT (wt-HDAC) and R6/2^{Q300} transgenic (Tg-HDAC) mice. The total number of gene expression changes for each condition is shown in parenthesis under each label.

Movie S1. Vehicle-treated WT mouse (6 months of age).

Movie S1 (MOV)

Movie S2. Vehicle-treated R6/2 transgenic mouse (6 months of age).

Movie S2 (MOV)

Movie S3. HDACi 4b-treated R6/2 transgenic mouse (6 months of age).

Movie S3 (MOV)

Table S1. Functions analysis of HDACi 4b-induced down-regulated genes in R6/2 transgenic mice

Cerebellum		Cortex		Striatum	
Function	*P* value	Function	*P* value	Function	*P* value
Molecular transport	1.25E-04–3.03E-02	Inflammatory disease	7.6E-05–2.27E-02	Post-translational modification	3.41E-04–3.41E-04
Hematologic system development and function	1.5E-04–3.03E-02	Immunologic disease	8.02E-05–2.56E-02	Cell morphology	3.93E-04–3.03E-02
Organismal survival	1.5E-04–3E-03	Developmental disorder	1.29E-04–2.27E-02	Cell dycle	6.13E-04–3.07E-02
Tissue development	1.5E-04–3.03E-02	Endocrine system disorders	1.29E-04–2.35E-02	Cancer	6.18E-04–3.03E-02
Cell death	4.74E-04–3.03E-02	Neurologic disease	1.33E-04–2.27E-02	Cell-to-cell signaling and interaction	6.18E-04–2.87E-02
Neurologic disease	4.74E-04–3.03E-02	Immune response	3.6E-04–2.27E-02	Cellular function and maintenance	6.18E-04–3.03E-02
Cellular assembly and organization	5.13E-04–3.03E-02	Cell-to-cell signaling and interaction	7.62E-04–2.27E-02	Gene expression	6.18E-04–2.95E-02
Cellular development	8.77E-04–3.03E-02	Nervous system development and function	7.62E-04–2.57E-02	Hematologic disease	6.18E-04–2.87E-02
Cellular compromise	9.13E-04–3.03E-02	Lipid metabolism	1.54E-03–2.35E-02	Respiratory system development and function	6.18E-04–2.87E-02
Drug metabolism	9.13E-04–3.03E-02	Cancer	1.84E-03–2.57E-02	Tissue morphology	6.18E-04–2.87E-02
Endocrine system development and function	9.13E-04–3.03E-02	Cell cycle	1.84E-03–2.43E-02	Lipid metabolism	7.4E-04–2.87E-02
Lipid metabolism	9.13E-04–3.03E-02	Drug metabolism	1.88E-03–2.27E-02	Small molecule biochemistry	7.4E-04–2.87E-02
Nervous system development and function	9.13E-04–3.03E-02	Gene expression	2.46E-03–2.57E-02	Cellular development	1.19E-03–2.87E-02
Small molecule biochemistry	9.13E-04–3.03E-02	Endocrine system development and function	2.61E-03–2.27E-02	Connective tissue development and function	1.25E-03–2.87E-02
Skeletal and muscular system development and function	1.37E-03–3.03E-02	Immune and lymphatic system development and function	2.61E-03–2.47E-02	Organismal development	1.71E-03–2.87E-02
Connective tissue development and function	1.61E-03–3.03E-02	Tumor morphology	2.61E-03–2.27E-02	Immunologic disease	4.17E-03–2.87E-02
Cellular growth and proliferation	2.01E-03–3.03E-02	Cell morphology	2.77E-03–2.27E-02	Nervous system development and function	7.62E-03–2.87E-02
Cancer	2.19E-03–3.03E-02	Cell death	2.98E-03–2.56E-02	Cell death	7.78E-03–2.87E-02

The functional analysis annotation tool was used in Ingenuity Pathways Analysis software (Ingenuity Systems).

Table S2. Primer sequences used for real-time PCR and ChIP assays

Gene ID	Transcript ID	Forward primer (5′- 3′)	Reverse primer (5′- 3′)
Real-time PCR			
Calml4	NM_138304	gttcctttcccaggaccaaa	aggcacctcatggacaccag
Aqp1	NM_007472	gcttgccattggcttgtctg	ttgagaagttgcgggtgagc
Cldn1	NM_016674	gcgacattagtggccacagc	agggcctggccaaattcata
Folr1	NM_008034	ccacgaacacaagccaggaa	cccaagttcggggaacactc
Clic6	NM_172469	gcacgacatcaccctcttcg	ggtctgcaggcttccgtttt
Enpp2	NM_015744	accaagcaaggggtgagagc	ggcagggaaagccactgaag
Agxt2l1	NM_027907	acggccacctgtcgtcatta	gcagtggatgggtcttcgtg
Mt3	NM_013603	acctgctcggacaaatgcaa	atttctcggcctctgccttg
Ccr6	NM_009835	atctttccgggtacgctcca	cgtggctcacagacatcacg
Mtf1	NM_008636	acgtgcagggctgtgagaag	gaatgtgcttccgcaggtca
Agt	NM_007428	ccggaacgacctcctgactt	aaaagggtgggcagcttgtc
Scn4b	NM_001013390	gagtggtgtggaaggttggtt	actggtcaccccgatttcc
Hprt	NM_013556	tgatgaaggagatgggaggcc	ccagcaggtcagcaaagaacttatagc
ChIP			
Calml4	NM_138304	accttgttcttgggcttcc	gaaactcagccaccagatcc
Aqp1	NM_007472	tctagagtgccagcctctgc	cgttgctctaataggctttgg
Cldn1	NM_016674	ggagagacacgaagggaagag	ctccgtggtggatgatgatg
Folr1	NM_008034	tgactggaagtgggtgatagc	aacacaggcttgcaacttcc
Clic6	NM_172469	agctctgggttagactctcagg	gaccagattctgcctcttcc
Enpp2	NM_015744	tctgtgatcgctgtgtttcc	ctgggtacagcccactgc

Other Supporting Information Files

Dataset S1
Dataset S2